

Electronic Supplementary Information

Agar/Carbon Dots Crosslinked Polyacrylamide Double-Network Hydrogels with Robustness, Self-Healing, and Stimulus-Response Fluorescence for Smart Anti-Counterfeiting

Shaowen Xie,^a Yin chen,^a Ziyu Guo,^a Yuecong Luo,^a Haihu Tan,^a Lijian Xu,^{a,b} Jianxiong Xu,^{a,b*} and Jie Zheng^c

^aHunan Key Laboratory of Biomedical Nanomaterials and Devices, College of Life Science and Chemistry, Hunan University of Technology, Zhuzhou 412007, P. R. China

^bNational & Local Joint Engineering Research Center of Advanced Packaging Materials Developing Technology, Hunan University of Technology, Zhuzhou, 412007, PR China

^cDepartment of Chemical and Biomolecular Engineering, The University of Akron, Akron, OH, 44325, USA

† Electronic supplementary information (ESI) available.

Contents

Fig. S1 HR-TEM image of (A) PCD-b and (B) PCD-g; (C) ^1H NMR spectra of CD-b, CD-g, PCD-b, and PCD-g.

Fig. S2 XPS spectra of (A₁) PCD-b, (B₁) PCD-g, and (A₂-B₃) their corresponding high-resolution XPS spectra of N 1s and C 1s.

Fig. S3 UV-Vis spectrum and the photoluminescence emission spectra of (A) PCD-b and (B) PCD-g aqueous solution (2 mM). Photoluminescence emission spectra of (C) PCD-b and (D) PCD-g aqueous solution under excitation with different wavelengths (the inset is the normalized photoluminescence emission spectra).

Fig. S4 Visual inspection of mechanical and fluorescent properties of both PCD-B_{1.0} gels and PCD-G_{1.0} gels enduring high compression up to 20 MPa.

Fig. S5 SEM images of (A) PCD-B_{1.0} gels and (B) PCD-G_{1.0} gels.

Fig. S6 Tensile stress-strain of agar/pAM DN gels, agar/pAM-CD-B_{1.0} gels, and pAM-PCD-B_{1.0} SN gels.

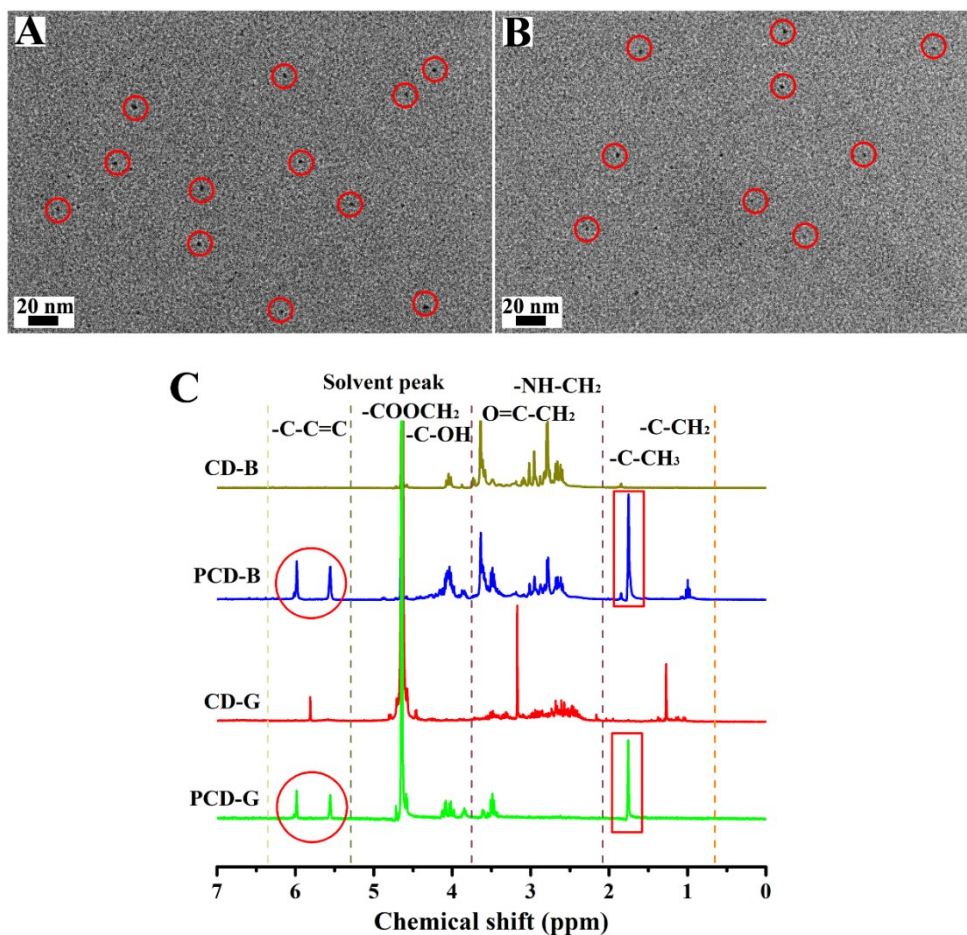
Fig. S7 (A-D) Hysteresis loops of PCD-B DN gels with different contents of PCD-b crosslinker at different strain using cyclic loading-unloading tests.

Fig. S8 (A-D) Hysteresis loops of PCD-G DN gels with different contents of PCD-g crosslinker at different strain using cyclic loading-unloading tests.

Fig. S9 Mechanical self-recovery of PCD-G_{1.0} gels using cyclic loading-unloading experiments, as indicated by hysteresis loops of PCD-G_{1.0} gels (A) without recovery time at 25 °C, with different resting times at (B) 25 °C and (C) elevated temperature of 95 °C, as well as (D) elastic modulus (stiffness) and (E) dissipated energy (toughness) recovery of PCD-G_{1.0} gels estimated from (B-C) curves.

Fig. S10 (A-D) Hysteresis loops of PCD-G DN gels with different contents of PCD-g crosslinker at different strain using cyclic loading-unloading tests.

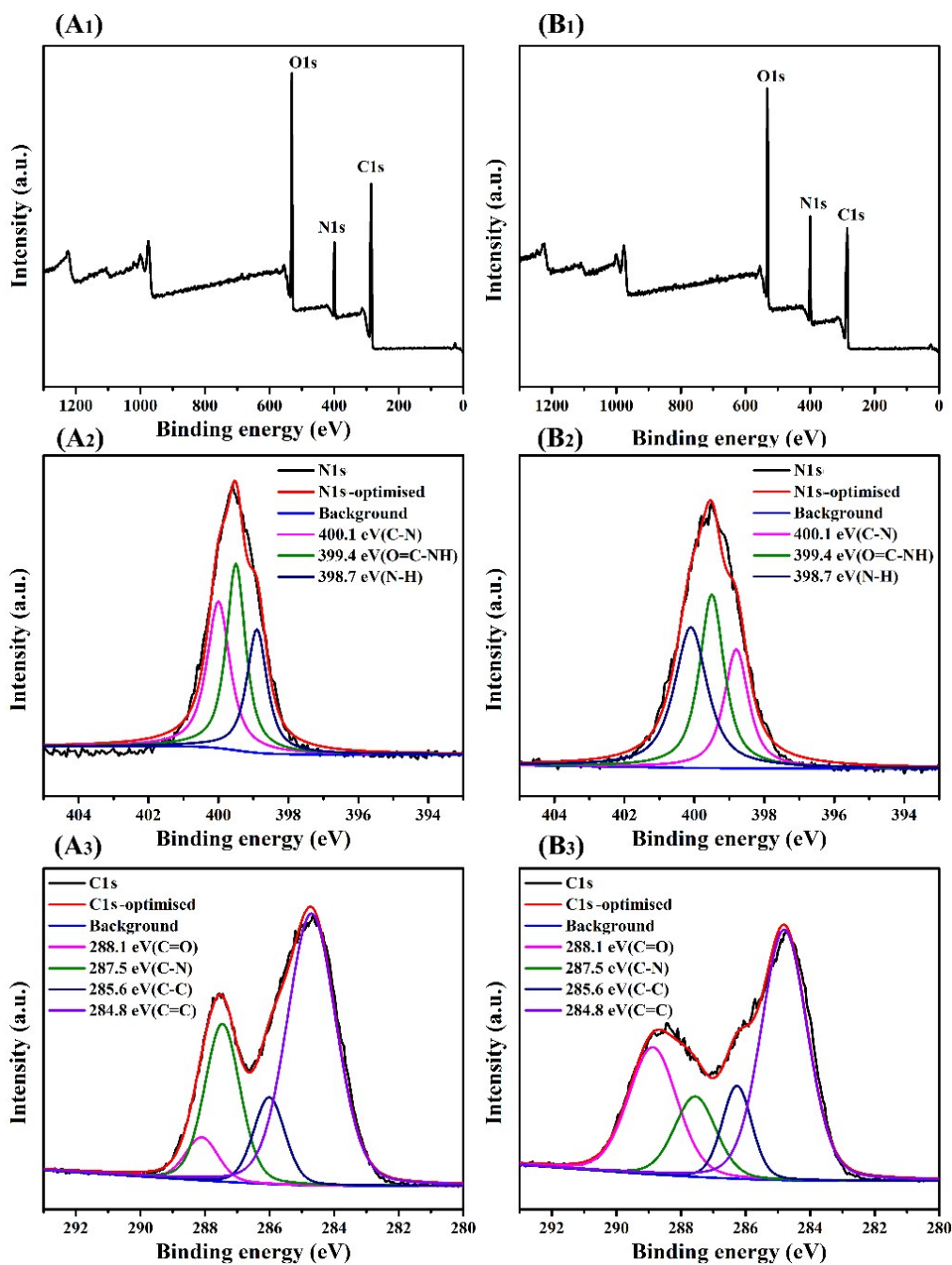
Fig. S1 HR-TEM image of (A) PCD-b and (B) PCD-g; (C) ¹H NMR spectra of CD-b, CD-g, PCD-b, and PCD-g.



The morphology of both PCD species was investigated by high resolution transmission electron microscopy (HR-TEM) as shown in **Fig. S1(A-B)**. It can be seen that both types of PCD exhibited homogeneously dispersed, and mostly in the form of spherical morphologies. The average size was about 3-4 nm estimated by the statistical analysis of the particles. Meanwhile, there was no lattice fringe can be seen in their HR-TEM images, demonstrating that both as-obtained PCD had an amorphous nature. Such small and well-dispersed nanoparticles could effectively minimize the steric hindrance effect, thus can be used as ideal crosslinker to copolymerize with hydrogel network. To examine whether both double-bond-functionalized

PCD were successfully synthesized by the reaction of amino groups on the CD surface with epoxy groups of glycidyl methacrylate molecules, all the four types of as-obtained carbon dots (CD-b, CD-g, PCD-b, and PCD-g,) were performed by ^1H NMR. As shown in **Fig. S1(C)**, the main proton resonance of all four carbon dots were located in the mid-field region between 3.0 to 5.0 ppm, which were assigned to the protons of $-\text{COOCH}_2$, $-\text{C-OH}$, O=C-CH_2 , and $-\text{NH-CH}_2$ functional group. More important, some new proton-resonance peaks were observed in the ^1H NMR spectra of PCD-b and PCD-g after surface modification. Among these proton-resonance peaks, the resonance at 6.0 and 5.6 ppm were assigned to the protons of $-\text{C-C=C}$ group. The resonance at 1.7 ppm were belong to the protons of $-\text{C-CH}_3$ group. The presence of all these new peaks indicated that glycidyl methacrylate molecule with terminal double bonds were successfully grafted onto the surface of CD.

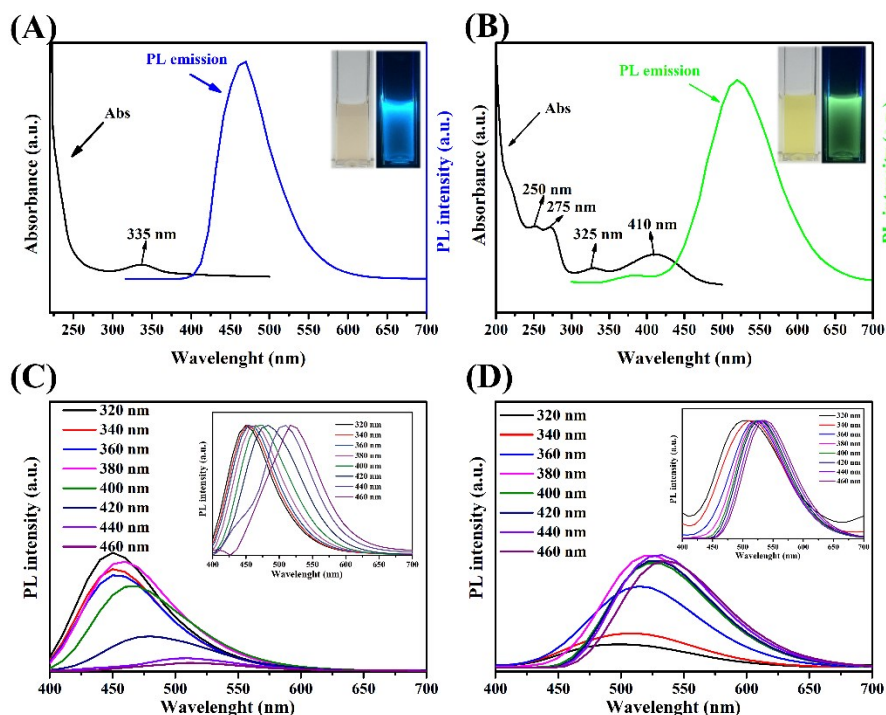
Fig. S2 XPS spectra of (A₁) PCD-b, (B₁) PCD-g, and (A₂-B₃) their corresponding high-resolution XPS spectra of N 1s and C 1s.



As shown in Fig. S2(A₁-B₁), two PCD species both exhibited three typical binding energy peaks at 285.0, 400.0, and 532.0 eV in their corresponding wide-scan XPS spectrum, which were attributed to C 1s, N 1s, and O 1s, respectively. All these peaks were confirmed presence of C, N,

and O elemental components in both PCD species. Furthermore, for both PCD species, their corresponding high-resolution XPS spectra of N1s can be curve fitted with three binding energy peaks at 398.7 eV, 399.4 eV and 400.1 eV, corresponding to N-H, O=C-NH, and C-N, respectively (**Fig. S2(A₂-B₂)**). In parallel, the high-resolution XPS spectra of C1s both contained four constitute of carbon bonds at 284.8, 285.6, 287.5 and 288.1 eV, which belonging to the PCD in the form of C-C, C=C, C-N, and C=O, respectively (**Fig. S2(A₃-B₃)**). These results combined with ¹H NMR results indicated that two PCD species were successfully prepared and such abundant functional groups on the surface of PCD were conducive to the photoluminescent performance.

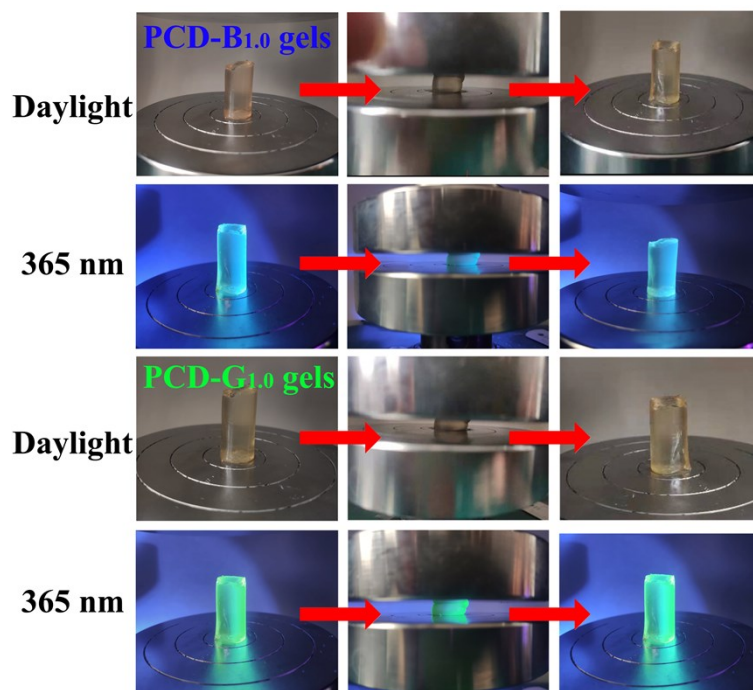
Fig. S3 UV-Vis spectrum and the photoluminescence emission spectra of (A) PCD-b and (B) PCD-g aqueous solution (2 mM). Photoluminescence emission spectra of (C) PCD-b and (D) PCD-g aqueous solution under excitation with different wavelengths (the inset is the normalized photoluminescence emission spectra).



With regard to optical properties, both PCD-b and PCD-g can be well dispersed into the aqueous solutions and exhibited no optical emission under daylight. However, PCD-b and PCD-g emitted distinct blue and green fluorescence under a 365 nm UV lamp, respectively (inset in **Fig. S3 (A-B)**). Moreover, UV-Vis spectrum of PCD-b exhibited an optical absorption band appeared at around at 335 nm, corresponding to $n-\pi^*$ transition of the C=O bonds (**Fig. S3A**). The absorption line of PCD-g had four peaks at about 250, 275, 325, and 410 nm. The peaks at 250 and 275 nm in the short wavelengths were attributed to unsaturated bond transitions of sp^2 domains, while broad absorption bands at 325 and 410 nm in the longer wavelengths would be corresponding to C-N bonds or the $n-p^*$ transition of the C=O bond from the surface structures (**Fig. S3B**). As

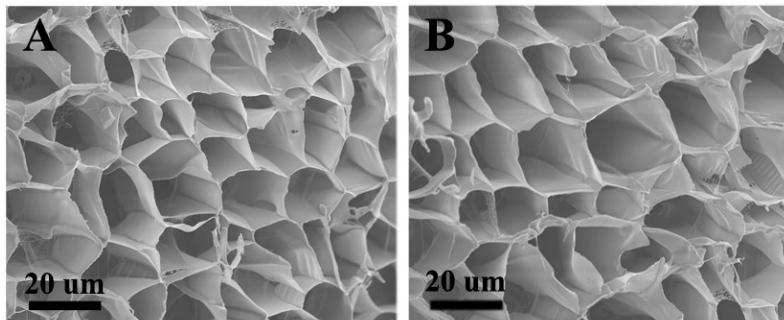
expected, upon excitation at 360 nm, the PCD-b aqueous solution showed strong blue emission with a peak at around 460 nm, while the PCD-g exhibited strong blue emission with a peak at around 540 nm. To further investigating the fluorescent properties of the as-prepared PCD, we also examined the photoluminescent behavior of PCD with different excitation wavelengths ranging from 320 to 460 nm. As shown in **Fig. S3(C-D)**, it can be seen that the best fluorescence intensity of PCD-b was around 450 nm at the excitation wavelength of 320 nm (**Fig. S3(C)**), while the maximum fluorescence intensity of PCD-g was around 525 nm at the excitation wavelength of 380 nm (**Fig. S3(D)**). Undoubtedly, both PCD-b and PCD-g revealed typical wavelength-dependent photoluminescence behavior, the photoluminescence peak of PCD-b red shifted from 450 to 520 nm by changing the excitation wavelength from 320 to 460 nm. Similarly, the maximum emission peak of PCD-g also red shifted from 500 to 540 nm by increasing the excitation wavelength from 320 to 460 nm. This excitation-dependent-emission phenomenon may be due to the different surface states of the PCD.

Fig. S4 Visual inspection of mechanical and fluorescent properties of both PCD-B_{1.0} gels and PCD-G_{1.0} gels enduring high compression up to 20 MPa.



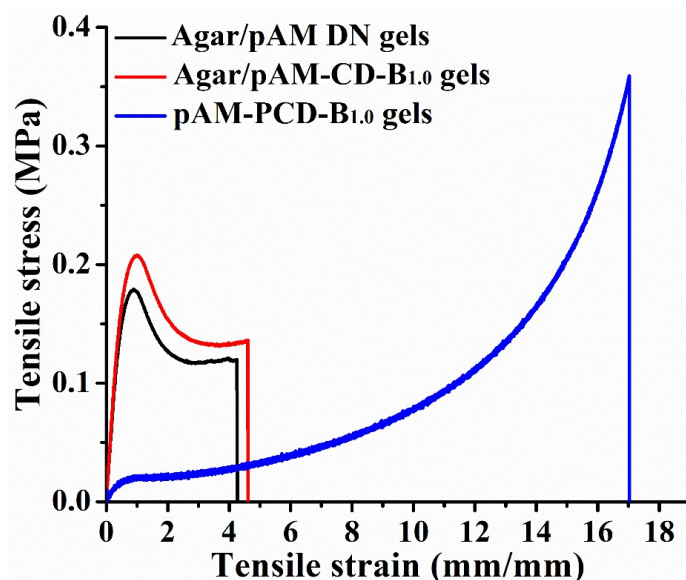
In parallel to tensile test, the mechanical and fluorescent properties both PCD-B_{1.0} gels and PCD-G_{1.0} gels were also evaluated by compression tests. As shown in **Fig. S4**, it can be seen that both PCD-B_{1.0} gels and PCD-G_{1.0} gels were able to endure high compression up to 20 MPa and maintain their original fluorescence.

Fig. S5 SEM images of (A) PCD-B_{1.0} gels and (B) PCD-G_{1.0} gels.



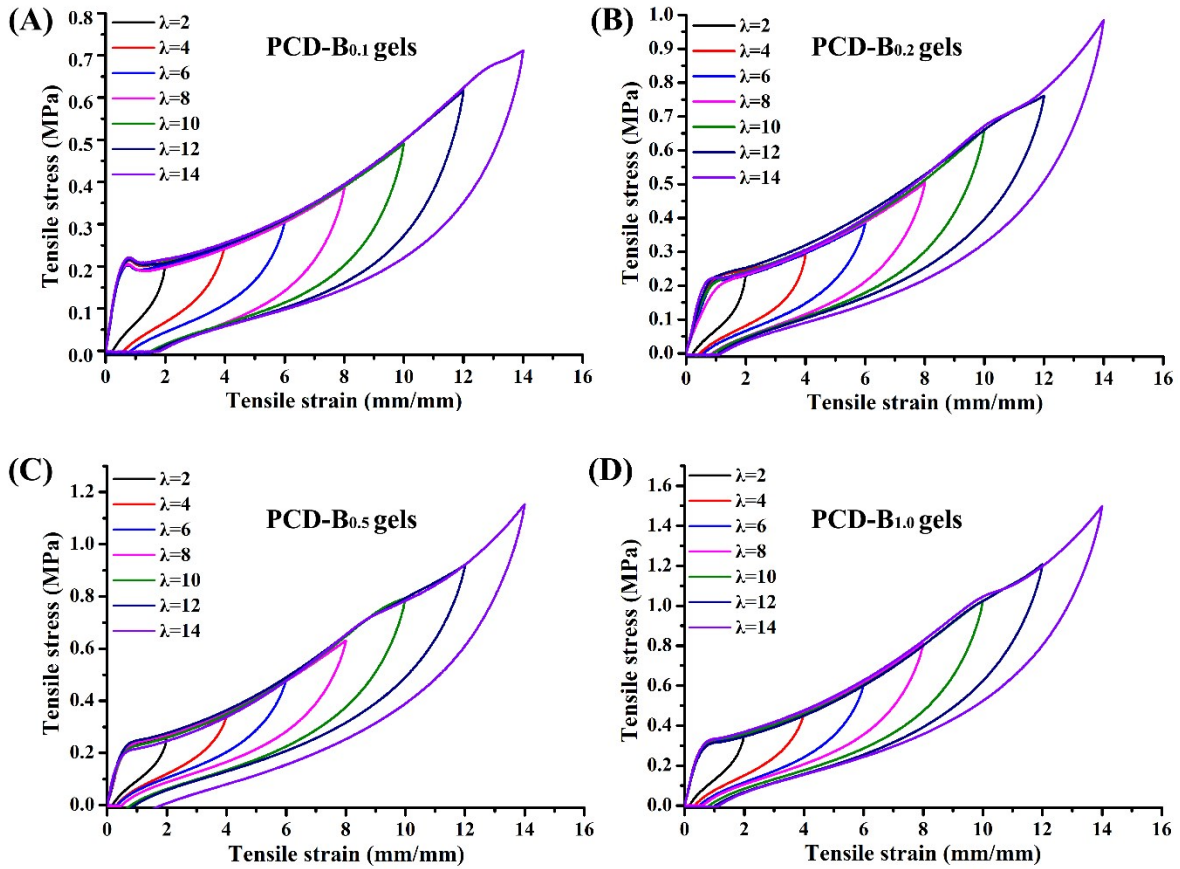
The interior network morphologies of both freeze-dried agar/pAM-PCD DN gels were checked by SEM. As shown in Fig. S5, the two hydrogels exhibited similar interior structure of densely interpenetrating networks and obviously porous characteristic, which were correlated with the excellent mechanical property of gels.

Fig. S6 Tensile stress-strain of agar/pAM DN gels, agar/pAM-CD-B_{1.0} gels, and pAM-PCD-B_{1.0} SN gels.



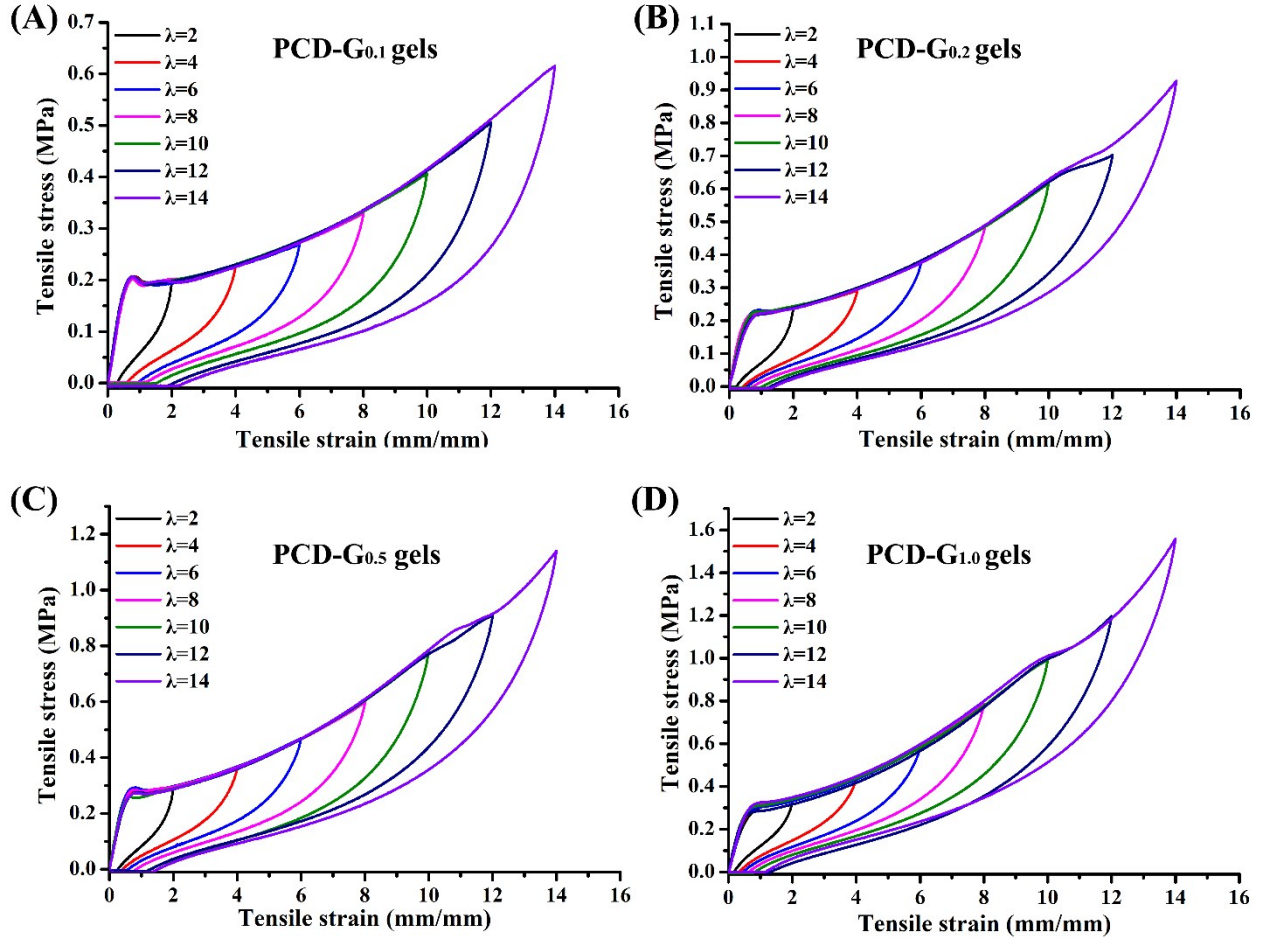
In order to demonstrate that PCD crosslinker and the interpenetrated physical/chemical crosslinked double network structure played important role in determine the mechanical properties of the agar/pAM-PCD DN hydrogels, three comparison samples of agar/pAM DN gels, agar/pAM-CD-B_{1.0} gels, and pAM-PCD-B_{1.0} SN gels were prepared and their mechanical properties were evaluated. As shown in **Fig. S6**, the agar/pAM gels without PCD crosslinker showed a tensile stress of 0.18 MPa at a tensile strain of 420%. Agar/pAM-CD-B_{1.0} gels showed a tensile stress of 0.20 MPa at a tensile strain of 460%. The pAM-PCD-B_{1.0} SN gels without the agar physical network also exhibited a low tensile stress of 0.36 MPa at a tensile strain of 1700%. All three comparison samples exhibited weak mechanical strength in comparison with the PCD-B_{1.0} gels (1.68 MPa at a tensile strain of 1400%). These results indicated that the PCD acted as cross-linker covalently crosslinked into the polymer framework and the formation of double network structure with chemical network interpenetrated through the agar physical network.

Fig. S7 (A-D) Hysteresis loops of PCD-B DN gels with different contents of PCD-b crosslinker at different strain using cyclic loading-unloading tests.



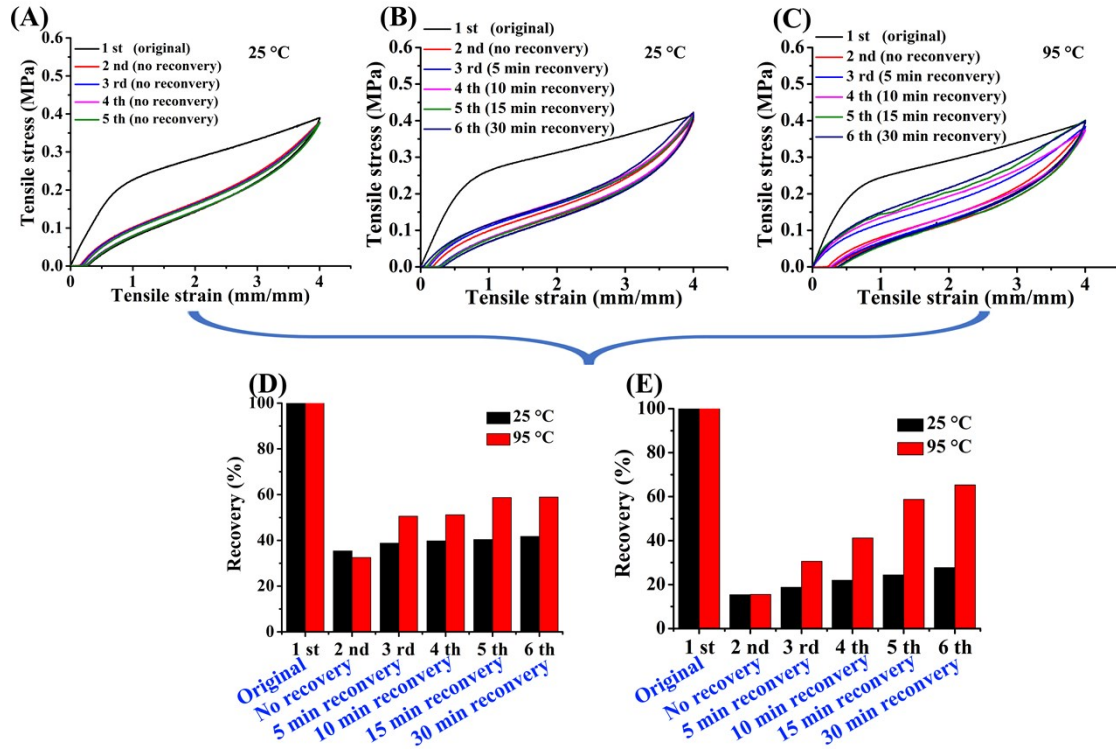
To understanding the role of PCD-b crosslinker on the dissipated energy of PCD-B DN gels, different cyclic loading-unloading tests were conducted on PCD-B DN gels at different strain. As shown in **Fig. S7(A-D)**, the cyclic loading-unloading curves of PCD-B DN gels with a continuous increase in the contents of PCD-b crosslinker and the tensile strain.

Fig. S8 (A-D) Hysteresis loops of PCD-G DN gels with different contents of PCD-g crosslinker at different strain using cyclic loading-unloading tests.



Similarly, the different cyclic loading-unloading tests of PCD-G DN gels were performed to study the role of PCD-g crosslinker on the dissipated energy of PCD-G DN gels. In parallel, the cyclic loading-unloading curves of PCD-G DN gels also continuous increased as increase in the contents of PCD-g crosslinker and the tensile strain (**Fig. S8(A-D)**).

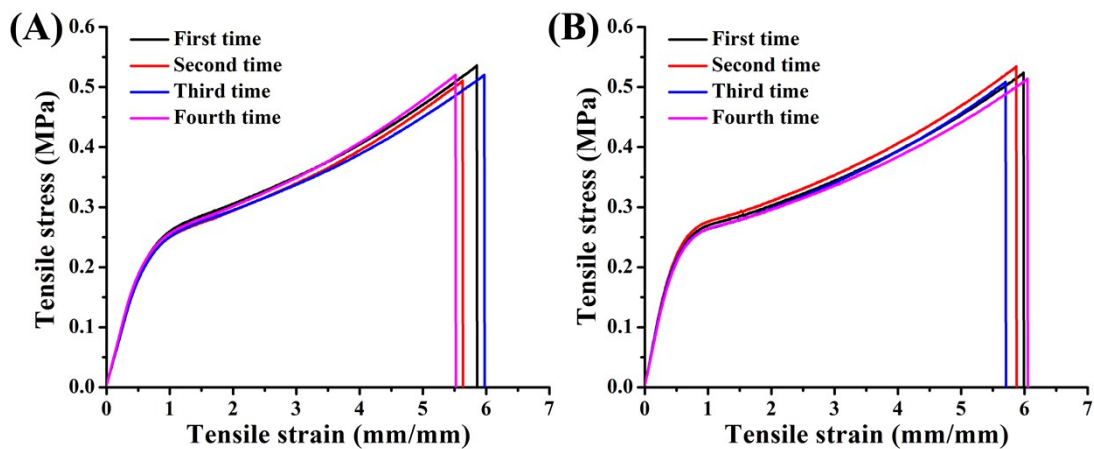
Fig. S9 Mechanical self-recovery of PCD-G_{1.0} gels using cyclic loading-unloading experiments, as indicated by hysteresis loops of PCD-G_{1.0} gels (A) without recovery time at 25 °C, with different resting times at (B) 25 °C and (C) elevated temperature of 95 °C, as well as (D) elastic modulus (stiffness) and (E) dissipated energy (toughness) recovery of PCD-G_{1.0} gels estimated from (B-C) curves.



In parallel to PCD-B_{1.0} DN gels, the self-recovery properties of PCD-G_{1.0} DN gels in dependence of resting times and temperature were evaluated by cyclic loading-unloading experiments. Firstly, PCD-G_{1.0} gels were performed by five loading-unloading cycles at a strain of $\lambda=4$ and 25 °C without any resting time between cycles. As shown in **Fig. S9A**, the PCD-G_{1.0} gels showed a large hysteresis loop with dissipated energy of 0.53 MJ/m³ in the 1st cycle, but displayed small hysteresis loops with a much smaller dissipated energy of 0.08 MJ/m³, indicating the network fracture of PCD-G_{1.0} gels cannot be recovered immediately without resting at 25 °C. Similarly, a series of loading-unloading cycles at 25 °C and 95 °C with different resting time between cycles

were also performed to investigate the self-recovery of the PCD-G_{1.0} gels. As shown in **Fig. S9(B-E)**, the hysteresis loops of the PCD-G_{1.0} gels were obvious difference under different temperature and their corresponding stiffness/toughness recovery rates were as low as 37.4%/18.5%, 37.8%/19.6%, 39.5%/21.5%, and 40.5%/23.6% after 5, 10, 15, and 30 min of resting time at 25 °C. However, the PCD-G_{1.0} gels also showed improved self-recovery properties at elevated temperature of 95 °C with stiffness/toughness recovery of 50.6%/30.6%, 51.1%/41.2%, 58.7%/58.7%, and 59.0%/65.3% after different heating time, respectively.

Fig. S10 Mechanical tensile tests on the self-healed (C) PCD-B_{1.0} gels and (D) PCD-G_{1.0} gels after different times of cutting/self-healing process at 95 °C for 12 h.



In addition, we further challenged the mechanical strength of both PCD-B_{1.0} gels and PCD-G_{1.0} gels after more times of cutting/self-healing process. As shown in **Fig. S10**, the mechanical strength of both self-healing PCD-B_{1.0} gels and PCD-G_{1.0} gels remained almost unchanged after four times of self-healing, indicating the good self-healing stability of agar/pAM-PCD DN hydrogels.